Proceedings of the ASME 2010 3rd Joint US-European Fluids Engineering Summer Meeting and 8th International Conference on Nanochannels, Microchannels, and Minichannels
FEDSM-ICNMM2010
August 1-5, 2010, Montreal, Canada

FEDSM-ICNMM2010-30833

THE DYNAMICS OF A CANTILEVERED PIPE ASPIRATING FLUID STUDIED BY EXPERIMENTAL, NUMERICAL AND ANALYTICAL METHODS

Dana Giacobbi
McGill University
Montreal, Quebec, Canada
dana.giacobbi@mail.mcgill.ca

Stephanie Rinaldi
McGill University
Montreal, Quebec, Canada

Christian Semler
McGill University, Simutech Group
Montreal, Quebec, Canada
csemler@simutechgroup.ca

Michael Païdoussis
McGill University
Montreal, Quebec, Canada
mary.fiorilli@mcgill.ca

ABSTRACT

This paper investigates the dynamics of a slender, flexible, aspirating cantilevered pipe, ingesting fluid at its free end and conveying it towards its clamped end. The problem is interesting not only from a fundamental perspective, but also because applications exist, notably in ocean mining [1]. First, the need for the present work is demonstrated through a review of previous research into the topic – spanning many years and yielding often contradictory results – most recently concluding that the system loses stability by flutter at relatively low flow velocities [2]. In the current paper, that conclusion is refined and expanded upon by exploring the problem in three ways: experimentally, numerically and analytically. First, air-flow experiments, in which the flow velocity of the fluid was varied and the frequency and amplitude of oscillation of the pipe were measured, were conducted using different elastomer pipes and intake shapes. Second, a fully-coupled Computational Fluid Dynamics (CFD) and Computational Structural Mechanics (CSM) model was developed in ANSYS in order to simulate experiments and corroborate experimental results. Finally, using an analytical approach, the existing linear equation of motion describing the system was significantly improved upon, and then solved via the Galerkin method in order to determine its stability characteristics. Heavily influenced by a CFD analysis, the proposed analytical model is different from previous ones, most notably because of the inclusion of a two-part fluid depressurization at the intake. In general, both the actual and numerical experiments suggest a first-mode loss of stability by flutter at relatively low flow velocities, which agrees with the results from the new analytical model.

1. INTRODUCTION

The dynamics of discharging cantilevered pipes, i.e. pipes that transport fluid from the clamped end to the free end, has been investigated thoroughly and continuously for nearly 50 years. The simplest linear model of this system, generally predicting flutter, has been well-established for years; it has even emerged as a paradigm in dynamics, a well-understood stepping stone for tackling more complex systems. Why, then, does the simple act of reversing the flow direction and causing the pipe to aspirate, i.e. to ingest fluid at the free end and convey it towards the clamped end, as shown in Fig. 1, spark so much interest, debate and controversy? In over 20 years, the aspirating cantilevered pipe has been studied experimentally, theoretically and numerically, yet the analysis has never yielded altogether conclusive, incontrovertible results.

The first attempt at understanding the dynamics of aspirating cantilevered pipes, motivated by an essentially fundamental interest, consisted of experiments carried out at the Chalk River Nuclear Laboratories of Atomic Energy of Canada in 1966 by Païdoussis [3], in which a pipe was submerged in water and made to ingest it. No instability was ever observed, and a shell-type buckling collapse, caused by the large transmural pressure near the clamped end, prevented an investigation of the behaviour at higher flow velocities. Reinforcement of the pipe at the location of collapse did not eliminate the problem, and the experiments were eventually abandoned.

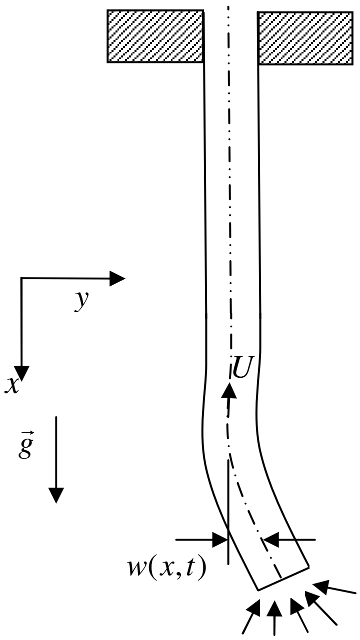

Figure 1. Schematic of an instantaneously deformed aspirating cantilevered pipe.

Several years later, an application for the aspirating cantilevered appeared in the deep ocean mining of minerals such as manganese nodules, prompting an analytical study of the system by Païdoussis & Luu [1]. Replacing $+U$ with $-U$ in the linear equation of motion for a cantilevered pipe discharging fluid, their analysis concluded that the aspirating pipe loses stability by flutter at very low flow velocities in general, and at infinitesimal flow velocities in the absence of damping. Unconvinced, in 1986 Païdoussis built a new experimental set-up at McGill University to revisit the problem [3]. However, flutter remained elusive and, eventually, a rather unfortunate freak accident – reminiscent of Richard Feynman's famous 'inverse sprinkler' mishap [4, 5] – brought about the premature abandonment of this pursuit.

Nonetheless, still dissatisfied with the apparent disagreement between theory and experiments, Païdoussis [6] re-evaluated the analytical problem, upon realizing that the flow field at the intake is not the mirror-image of the discharging case. In other words, the fluid does not enter the pipe as a reverse jet, as had effectively been assumed in 1985; rather, Païdoussis now assumed a sink-like flow. In this case, the inlet gauge pressure is not zero. Instead, the sudden velocity increase causes a mean depressurization at the inlet, $\overline{p}_{\text{inlet}} = -\rho U^2$, where ρ is the density of the fluid and U is the mean flow velocity inside the pipe, effectively cancelling out the centrifugal force in the equation of motion, and eliminating the potential for flutter. Moreover, almost simultaneously, renewed experiments involving two flexible elastomer pipes fitted with plastic elbows at their free ends and interconnected by a pump at their clamped ends appeared to confirm the cancellation of the centrifugal force and the impossibility for flutter to arise.

Later, Kuiper & Metrikine [7] argued that Païdoussis was overvaluing the inlet depressurization, and therefore that the conclusion reached was incorrect. They suggested that the depressurization should instead be somewhere between $-\rho U^2$ and $-\frac{1}{2}\rho U^2$, the latter found using Bernoulli's equation, and that, as a result, the centrifugal force may not be wholly cancelled out. Furthermore, they reasoned that, even in the absence of the centrifugal force, the Coriolis force generates negative damping in the case of an aspirating pipe, and thus the system may lose stability after all. Finally, it was their assertion that the substantial drag caused by the surrounding fluid, water, was what prevented the occurrence of flutter in experiments, rather than the fundamental dynamics of the system.

Soon after, a theoretical reappraisal of the problem was undertaken by Païdoussis *et al.* [8], the two key new assumptions being that (i) rather than a pure sink-flow, there exists a small (but non-zero) mean flow velocity, v, just facing the inlet and (ii) there exists an additional mean tension at the free end of the pipe, related to the flow over the inlet lip (edge) of the pipe and the factor $\gamma = \overline{p}_{\text{edge}} / \overline{p}_{\text{inlet}}$. Under these assumptions, two variants of the model were considered [9]. In the first, v remains vertical during the motion of the system, whereas in the second, v always remains tangential to the free end. In the first case, the pipe always remains stable, as before. In the second case, the aspirating pipe can become subject to flutter, but even qualitative results are dependent on the values chosen for v and γ. It therefore became crucial to obtain accurate estimates of these quantities, and a CFD analysis was initiated to elucidate the inlet flow dynamics.

Giacobbi *et al*. [2] carried out the CFD analysis and established values for v and γ, concluding that the aspirating pipe can indeed flutter. This result was corroborated, at least qualitatively, by preliminary experiments with air, and by a coupled numerical CSM-CFD analysis in ANSYS which replicated experiments as faithfully as possible at the time. However, quantitatively, agreement between analytical results, experiments and numerical experiments remained unsatisfactory, and therefore so too did a unified, cohesive theory.

At about the same time, Kuiper *et al.* [10, 11, 12] renewed efforts to capture the instability, if it exists, in experiments. In order to accomplish this, a 5 m long aspirating pipe was only *partly* submerged in a large tank filled with water, therefore greatly reducing the viscous drag as compared to previous experiments. Under these conditions, they found that the aspirating pipe does appear to lose stability above a certain critical flow velocity, and that the motion is an unpredictable sequence of (i) nearly periodic orbital motions and (ii) noise-like vibrations of small amplitude. However, similarly to Giacobbi *et al*., in comparing their results with existing theory, they found that neither the critical flow velocity for flutter nor the behaviour of the pipe in the unstable region could be predicted.

The aspirating cantilevered pipe has perplexed researchers for many years, and continues to draw interest from a purely fundamental perspective. However, as new applications emerge in processes such as ship-board natural gas liquefaction and gas hydrate exploitation, a better understanding of this system has moved from being desirable to necessary. Therefore, the present paper has two objectives: (i) to strengthen the conviction that aspirating cantilevered pipes can be subject to flutter, by presenting new numerical and experimental evidence to support it, and (ii) to present a new linear theory, based on results from CFD analysis and new physical insight, that better explains the observed behaviour and provides additional insight into the fundamental dynamics of the system.

2. EXPERIMENTAL INVESTIGATION

The uncertainty plaguing past results and the unsatisfactory nature of the available evidence were convincing enough reasons to warrant a renewed interest in experiments. In particular, though unstable behaviour had most recently been witnessed by Kuiper *et al.* [10], Kuiper and Metrikine [11], and Kuiper [12], the small amplitude and irregular nature of the motion were cause for uncertainty; substantiation was therefore highly desirable.

The new experiments were distinct from earlier ones mainly in that, building on the preliminary experiments carried out by Giacobbi *et al* (2), they were conducted using air-flow entirely. Earlier experiments using water, in which the pipe was therefore immersed in water, were problematic for two reasons. Firstly, and most importantly, as pointed out by Kuiper and Metrikine [7], the considerable drag induced by the surrounding water would dampen out any small oscillations if they should arise. Secondly, at high flow velocities, a shell-type buckling collapse would occur near the clamped end of the cantilevered pipe due to a large transmural pressure difference. Using air-flow, both these issues were circumvented entirely.

2.1 EXPERIMENTAL APPARATUS

The experimental apparatus allowed for a controlled air feed to either the clamped end or the free end of the pipe, and measurement of the amplitude of pipe motion. In particular, it included (i) a large steel tank, (ii) an internal plexiglas flow-guiding protective conduit, (iii) a flexible elastomer pipe, and an Optron system for measuring displacements.

The tank intake/outlet connections could easily be reconfigured to accommodate either a discharging or an aspirating pipe. As shown in Figs. 2(a) and 2(b), the discharging configuration was obtained by feeding air to the clamped end directly, whereas aspiration was instead achieved by feeding air into the tank, thereby pressurizing it and forcing air up the pipe. The tank also possessed a plexiglas window for both viewing and recording purposes, and three pressure gauges located at different locations to monitor fluid characteristics.

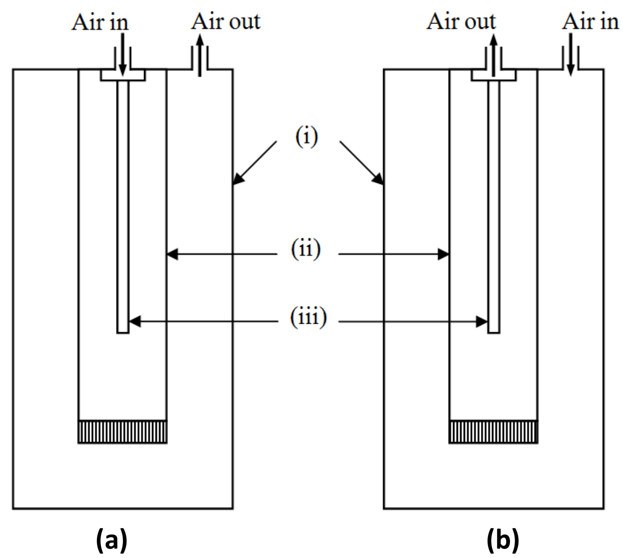

Figure 2. Experimental set-up; **(a)** discharging configuration; **(b)** aspirating configuration. (i) large steel tank, (ii) plexiglas protective conduit, and (iii) flexible elastomer pipe.

The protective 15 cm × 15 cm conduit was used to reduce flow disturbances and eliminate cross-flow that would otherwise interfere with the motion of the pipe and produce inaccurate results; it was placed within the tank and attached to the top cover of the latter by bolts. The combination of two screens and a honeycomb grid were placed at the lower end of the conduit to slow down and regularize the incoming flow. In this way, the air surrounding the pipe would be, for the most part, quiescent.

Finally, an Optron system, which is a non-contact electro-optical biaxial displacement follower system, was employed together with LabVIEW to acquire a time history of the motion of the pipe at various flow velocities. The amplitude and frequency of the pipe motion were obtained from these time histories.

For complete details and additional figures regarding the experimental apparatus, the reader is referred to Rinaldi [13].

2.2 EXPERIMENTAL PIPES

The experiments were performed using three different flexible elastomer pipes, fabricated in-house, using *Silastic*® E RTV Silicone Rubber from Dow Corning. Each pipe had distinctive defining characteristics, as follows: (i) Pipe 1 was an ordinary elastomer pipe without any special attributes; (ii) Pipe 2 was constrained to move in a 2-D plane by inserting a thin metal blade along its length during the casting process; (iii) Pipe 3 was made denser by introducing fine copper particles within the silicone rubber mixture. The specific geometrical and physical characteristics of Pipe 1 are presented in Section 5 when comparing with theory.

In addition to their defining characteristics, each pipe could be fitted with differently profiled end-pieces, whose purpose was two-fold. Firstly, the end-piece would prevent – or at least delay – a shell-type flutter instability and subsequent collapse at the free end of the pipe, observed to otherwise be inevitable at high aspirating flow velocities*. Secondly, the various end pieces would provide differing intake profiles, in order to help elucidate the effect of the intake flow dynamics on the overall stability of the system. The simplest end-piece, 1A, used to produce the results given in the present paper, offered a straight cylindrical intake.

It should be mentioned that, given the similarity between results discussed in Section 2.4, a full description of the different pipe characteristics and end-pieces is not warranted in this paper. Therefore, for details, the reader is referred to Rinaldi [13].

2.3 EXPERIMENTAL VALIDATION

To verify the capabilities and effectiveness of the apparatus, it was first tested under the discharging configuration, for which comparison with well-established theory is easily achievable. The apparatus could not produce pipe flow velocities below 60 m/s – a minor nuisance – but consistently successfully yielded critical flow velocities, $U_{\text{crit}} \approx 120-130$ m/s, no more than 5 to 10% greater than those predicted by theory ($U_{\text{crit}} \approx 115$ m/s), an entirely acceptable difference for experiments of this type.

However, several uncommonly encountered factors became apparent during these preliminary tests, and deserve mention, as they may slightly influence the experimental aspirating dynamics. First, compressibility effects for Mach numbers approaching 0.5 were accounted for through standard iterative means for average quantities, but may have had minor local effects. Second, a pressure drop due to friction resulted in a slight change in fluid density from pipe end to pipe end, but, in calculations, an effective average density was considered to apply along the length of the pipe. Finally, in the case of the aspirating pipe only, the tank must be pressurized to varying extents to generate the reverse flow, causing the fluid density to become a weak function of flow velocity; however, in cases of comparison with theory or numerical simulations, computations were carried out based on an average density for the entire range of flow velocities.

* The first occurrence of this incredibly loud and still poorly understood event was wholly unexpected, scaring the lead author witless and leaving him to contemplate the solidity of a 1in plexiglas window.

2.4 EXPERIMENTAL RESULTS FOR THE ASPIRATING PIPE

Overall, the experimental results suggest that aspirating pipes are indeed subject to flutter, at smaller flow velocities than the discharging case: i.e. at $U \approx 60-100$ m/s for the aspirating case versus $U \approx 120$ m/s for the discharging case. In general, pipe motion was recorded for any flow velocity considered, with the lower bound of 60 m/s being imposed by the apparatus rather than the physical system. Moreover, as the flow velocity was increased, a steady increase in amplitude would follow and noticeably steepen. Fig. 3(a) illustrates this behaviour for Experiment 1A, i.e. Pipe 1 with end-piece A. However, similar to the experimental results obtained by Kuiper *et al.* [10], the motion was irregular, switching between appreciable orbital oscillations one minute, to a near negligible shuddering motion the next. The representative time history signal in Fig. 4 demonstrates this inconsistent yet recurring behaviour, which also explains the significant difference between the time-averaged rms amplitude and max amplitude values in Fig. 3(a). In Fig. 3, u is the dimensionless flow velocity, formally defined in Eq. (16), but also here for convenience: $u = (M/EI)^{1/2} UL$, where M is the mass of the conveyed fluid per unit length, U the flow velocity, and EI and L the flexural rigidity and length of the pipe respectively.

The motion was visibly in the first beam-mode of the pipe, a fact confirmed by the frequency results. When estimated with a simple chronometer, the frequency of oscillation remained nearly constant, though with a slow decrease apparent as the flow velocity is increased, as shown in Fig. 3(b). When calculated using the Optron and processed in MatLab, the result was essentially the same, but with several small frequency jumps recorded as the flow velocity was increased. It is reasonable to suggest that these jumps are not a physical reality, but instead an artefact of an analysis that could only provide discrete values of frequency and not a continuum.

Qualitatively, the substitution of one pipe for another or the addition of a profiled end-piece did not change the results. In general terms, the maximum amplitudes observed ranged from less than 1 mm (as small as 0.1 mm for the rms amplitude) at $U \approx 60$ m/s, to nearly 20 mm (or just over 5 mm for the rms amplitude) at $U \approx 150$ m/s. The conversion factor from dimensionless to dimensional flow velocity was calculated on a per run basis, and was based on an average fluid density taken over the entire run; generally $U/u \approx 20-25$ m/s. The observed frequency was approximately $f \approx 1.0-1.2$ Hz for all cases, though universally following the trend presented in Fig 3(b).

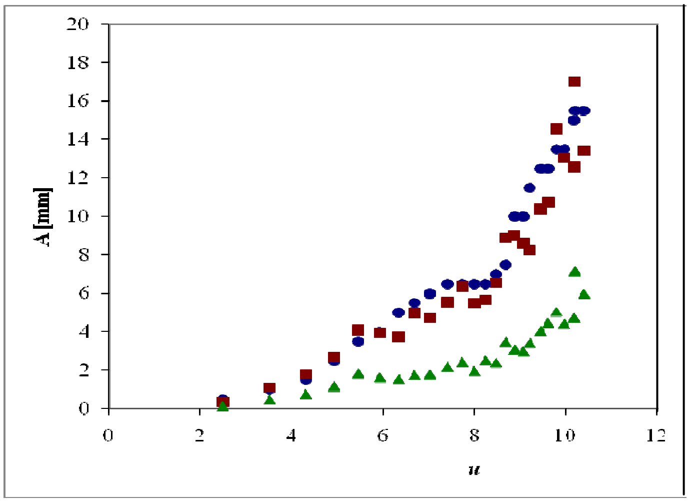

(a)

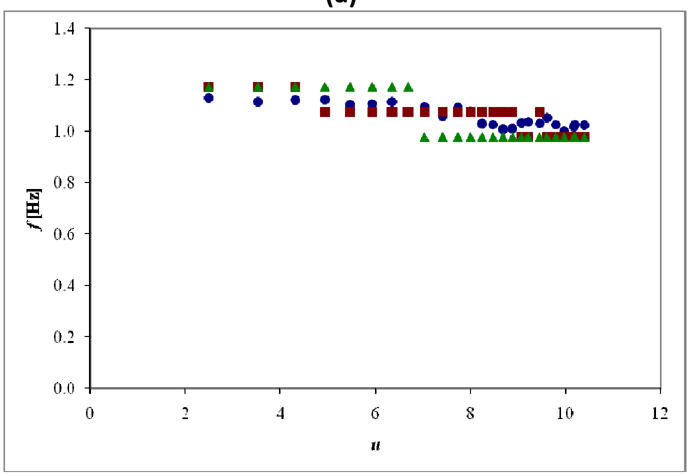

(b)

Figure 3. Typical experimental results, with displacements measured 5 mm above the free end of the pipe. **(a)** amplitude versus u: ● ruler estimate, ■ max amplitude, ▲ rms amplitude; **(b)** frequency versus u: ● chronometer estimate, ■ PSD (8 windows), ▲ PSD (16 windows).

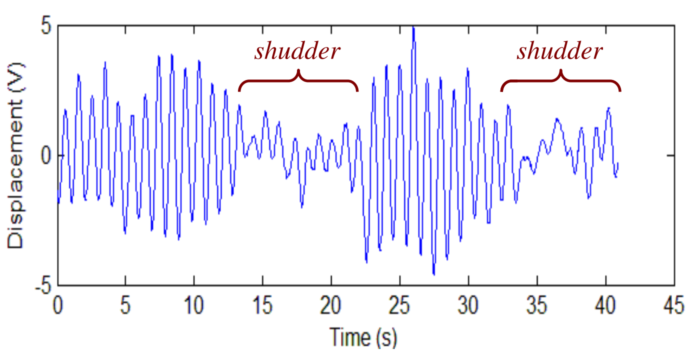

Figure 4. Typical time history signal for experiments, for $u = 11.0$, illustrating the characteristic shuddering motion commonly encountered during experiments.

At high flow velocities, the shell-type flutter and eventual shell-type collapse mentioned in Section 2.2 would take hold and put an end to the experiment. Without any end-piece, this instability would appear for flow velocities nearing $U \approx 120\,\text{m/s}$. Unfortunately, the addition of an end-piece would only delay the effect, allowing for flow velocities nearing $U \approx 150\,\text{m/s}$, but not prevent it.

Despite the evidence that the observed oscillation is a dynamic instability, the motion was considerably different from flutter of a typical discharging pipe. First, there is no sudden jump in amplitude, as there is with the discharging cantilever; rather the bifurcation curve follows a gradual increase. Second, the motion is irregular and inconsistent, switching between appreciable amplitude and a nearly quiescent phase irregularly. Third, and perhaps most important, the amplitude is, all things considered, quite small. All this prompts the inevitable question: is what we are witnessing in these experiments actually flutter?

In light of this troubling uncertainty, corroboration through numerical experiments became highly desirable, and is the subject of the next section.

3. NUMERICAL SIMULATIONS

The purpose of the numerical simulations was to capture the instability, if it exists, in a more controlled setting, and corroborate the not yet altogether certain conclusion drawn from experiments that aspirating cantilevered pipes can flutter. Numerical simulations involving a fully coupled ANSYS CSM-CFD model were therefore initiated by Giacobbi *et al.* [2], who found that flutter did, in fact, emerge after a certain threshold flow velocity was reached.

However, the validity and sufficiency of the results in [2], though qualitatively interesting and not to be dismissed, can be brought into question for several reasons, as follows: (i) the pipes used in numerical simulation possessed unrealistic physical characteristics, most importantly a very large visco-elastic damping and a very small Young's modulus and density; (ii) due to (i), direct corroboration of experiments was very difficult to obtain, even in non-dimensional terms; (iii) several simulation convergence criteria may have been insufficiently strict; (iv) displacements of over 0.02 m could not be captured due to mesh deformation limitations related to the inadequate mesh stiffness equation implemented.

3.1 NUMERICAL SIMULATION METHODOLOGY

The basic elements of the simulation methodology used in the current work are identical to those proposed by Giacobbi *et al.* [2]; refer also to Giacobbi [14]. To summarize, the pipe structure is modelled using finite elements in ANSYS Mechanical, and the internal and surrounding fluid is modeled in ANSYS CFX. A finite period of time and time step, structural and fluid properties, and boundary conditions are prescribed; the total behaviour is then observed as the simulation progresses in real time. The interaction between fluid and solid is computed at the interface, where CFX sends forces to and receives displacements from ANSYS Mechanical. The communication between the two is continued until the desired convergence criteria are met for both sides and even more importantly for the load transfer itself, at each timestep. Altogether, the fully-coupled CSM-CFD model replicates experiments by simulating an aspirating cantilevered pipe submerged in air.

The present work investigated the behaviour of two pipes. The first one, Pipe A, possessed realistic geometric and physical properties when compared to experiments, with the exception of density, which was again quite low. The second one, Pipe B, was a near-exact model of the experimental Pipe 1 from Table 1, save for two distinctions: (i) the fluid was not modelled as an ideal gas with variable density, and therefore was not subject to compressibility effects, and (ii) the hysteretic damping , $\bar{\mu}^*$, which is not available in ANSYS, was not modelled. Instead, the air density was set to a constant 1.18 kg/m^3, and an equivalent total viscoelastic damping was deduced by directly matching the decay of oscillations in numerical simulations to experiments. The effect of using a constant density should, in non-dimensional terms, be relatively small. Moreover, the effect of using an equivalent viscoelastic damping instead of a combined hysteretic-viscoelastic damping should also be small for the needs of this analysis, even in dimensional terms. Altogether, by being much more similar to experiments, these two cases – and particularly Pipe B – could be used to provide a much better test of agreement with experimental results. The specific geometrical and physical properties of Pipes A and B are presented in Section 5, when comparing with analytical results and experiments.

In order to verify whether the approach was viable, a discharging pipe was simulated and the critical flow velocity obtained was compared with theory, and in the case of Pipe B, also with experiments. The emergence of flutter was well predicted. Qualitatively, a classical bifurcation curve emerged: negligible or no motion at low flow velocities, and a rapid jump to large and often unattainable limit cycles at higher flow velocities. More specifically, the non-dimensional critical flow velocities were found to be within 10% of the theoretical ones for Pipe A, and within 5% of both the experimental and theoretical ones for Pipe B. These results were obtained with relative ease despite dimensional flow velocities surpassing 100 m/s, suggesting that these numerical experiments could be a viable means of simulating even a realistic aspirating pipe.

3.2 NUMERICAL SIMULATION RESULTS FOR THE ASPIRATING PIPE

Predictably, simulation of the aspirating cantilevered pipe proved to be a much more demanding undertaking. The challenges of using a more realistic pipe, avoided by Giacobbi *et al.* (2) at the expense of satisfactory corroboration, became clear when the necessarily higher flow velocities invariably translated into significant convergence difficulties. More specifically, unlike the discharging pipe where one force acting exclusively on the inner wall of the pipe generally dominates, the aspirating pipe is subject to competing forces on the inner pipe wall and at the free end. These forces tend to partially cancel each other out, such that the aspirating pipe is quite sensitive to any inaccuracy in the computations; in particular, even the effect of viscous damping due to the surrounding air becomes relatively important, whereas it plays a negligible role for the discharging case. Given the history of disagreement surrounding the aspirating cantilevered pipe, this sensitivity came as no revelation, but it nevertheless made obtaining completely satisfactory results difficult.

To begin with, Pipe A proved the easier to analyze. First, a reduced stiffness relaxed the necessity for elevated flow velocities and facilitated numerical convergence. In addition, and perhaps more importantly, a diminished density increased the relative importance of the flow velocity *vis-à-vis* amplitude, making the relationship between increasing amplitude and increasing flow velocity more obvious. Despite these advantages, obtaining clear-cut limit cycle oscillations proved difficult. The rate of energy flow into the system is evidently slow, resulting in slow convergence to the phase-plane trajectories towards a definite limit cycle. Instead, therefore, for each flow velocity, lower and upper bounds were estimated for the amplitude of the anticipated limit cycle oscillation. To accomplish this, initial perturbations of differing strengths were applied to the pipe aspirating at a given flow velocity, and the motion carefully observed for several cycles of oscillation. Generally, the amplitude of oscillation would either consistently increase or decrease, indicating a lower or upper bound respectively. By carrying out many such simulations, an approximate bifurcation curve was obtained, as shown in Fig. 5, in which the estimated amplitude is plotted versus flow velocity.

Subsequently, the more important case, Pipe B, was analyzed. A similar approach as with Pipe A was sought, but clean results remained elusive. More concretely, for a given flow velocity, when given no initial perturbation, the pipe would always begin to oscillate at a small, yet very slowly increasing amplitude. For the same flow velocity, when given a small initial push, the pipe would then generally begin to oscillate at an essentially constant amplitude, determined by the size of the push, exactly like a frictionless pendulum. Eventually, in some cases, a large enough perturbation would create an initial amplitude that the fluid flow could not sustain, and the pipe motion would begin to decay, though again very slowly. Specifically, for flow velocities below approximately $U \approx 70$ m/s (in dimensionless terms, $u \approx 2.5$), the range between the lower and upper bound was extensive to the point that estimating the anticipated limit cycle oscillation amplitude was unfeasible. Even more distressing, for higher flow velocities, the upper bound was altogether impossible to determine! In light of this, it was proposed that no perturbation be given, and that instead the simulations be left to run long enough that the slowly increasing amplitudes eventually reach a limit cycle, so as to finally obtain the elusive bifurcation curve. Unfortunately, the relatively low frequency of oscillation, the necessity for a small timestep and the difficulties associated with convergence in spite of everything, meant that a single run could potentially require months of computation time. Instead, a *minimum amplitude*† bifurcation curve was obtained, given in Fig. 5. This curve most definitely suggests an emerging instability, with amplitudes on the same order as the time-averaged rms amplitudes seen in experiments for the same pipe. With such a curve, the critical flow velocity was estimated by observing at which point the slope steepened and extrapolating.

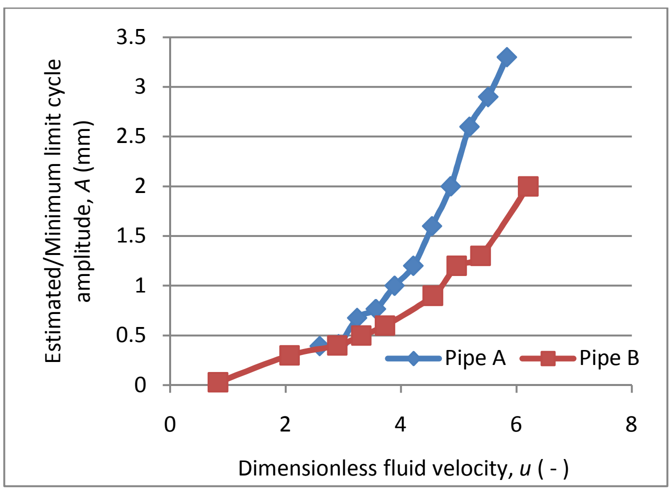

Figure 5. Aspirating bifurcation curves captured in numerical simulations. **Pipe A**: estimated limit cycle amplitude; **Pipe B**: minimum limit cycle amplitude.

For both pipes, the frequency results were essentially the same as what was found by Giacobbi *et al.* [2], and therefore are not elaborated upon here. In summary, similarly to experiments, the oscillation frequency is that of the first beam-mode and, as the flow velocity is increased, the frequency tends to decrease very slightly. Again, this is reminiscent of a pendular motion, and it would not be characteristic of flutter were it not for the non-negligible increasing amplitude previously described.

† The minimum amplitude here refers to the amplitude of the first peak observed during the motion of the pipe when no initial perturbation is given. The actual limit cycle is far greater; however, to obtain a reliable and consistent baseline for comparison, it is always this *minimum amplitude* which was considered rather than any other.

When taken together, these numerical simulation results do seem to indicate a flutter instability appearing at low flow velocities. However, as the numerical study of Pipe B most clearly demonstrated, this is an excessively weak instability – completely dissimilar to the sharp amplitude rise most often seen with the discharging cantilever. In fact, rather than flutter, in the case of a reasonably heavy and stiff pipe, the motion resembles that of an undamped pendulum. However, it is there: the fact that the motion does not ever damp out completely indicates that the flow is feeding energy into the system, and that that energy is sufficient to counteract the viscous and viscoelastic damping, and maintain a certain amplitude. Finally, when paired with the earlier results of Giacobbi *et al.* [2] that appeared to indicate a much sharper bifurcation for unrealistic pipes, it now seems clear that the numerical simulations agree with experiments in predicting that aspirating cantilevered pipes can and do, indeed, flutter.

4. THEORETICAL ANALYSIS

The new evidence presented in the foregoing suggests that perhaps a new attempt should be made to obtain a sound analytical model. However, the current work does not present a full derivation of the model; rather it focuses on new insights brought forth by the CFD analysis, the assumptions that have consequently been made and the ensuing results.

4.1 NEW THEORETICAL MODEL

The system under consideration consists of a uniform pipe of length L, flow area A, mass per unit length m, and flexural rigidity EI, conveying a constant property fluid of mass per unit length M, with constant mean axial flow velocity U from the free end to the clamped end, as illustrated in Fig. 1. The flow is assumed to be fully developed and turbulent. Furthermore, it is assumed that the pipe is slender, i.e. is long compared to the diameter, and undergoes only small lateral motions $w(x,t)$, where x is in the axial direction (with origin at the clamped end) and t is time. Under these assumptions, and without yet considering the effect of the intake dynamics, the simplified linear equation of motion can be gleaned directly from the equation for a discharging cantilever as originally derived by Païdoussis & Issid [15], and is

$$\begin{aligned} &EI\left[1+\left(\bar{\alpha}+\frac{\bar{\mu}^*}{\Omega}\right)\frac{\partial}{\partial t}\right]\frac{\partial^4 w}{\partial x^4}+ \\ &\left[MU^2-\left(\bar{T}-\bar{p}A\right)-\left(M+m-M_{\mathrm{a}}\right)g\left(L-x\right)\right]\frac{\partial^2 w}{\partial x^2} \\ &-2MU\frac{\partial^2 w}{\partial x\partial t}+\left(M+m-M_{\mathrm{a}}\right)g\frac{\partial w}{\partial x} \\ &+c\frac{\partial w}{\partial t}+\left(M+m+M_{\mathrm{a}}\right)\frac{\partial^2 w}{\partial t^2}=0. \end{aligned} \quad (1)$$

Here, $\bar{\alpha}$ is the Kelvin-Voigt type viscoelastic damping, $\bar{\mu}^*$ is the hysteretic damping [16], Ω is the circular frequency of oscillation, $\bar{T}$ is an external tension, $\bar{p}$ is an external pressurization, M_{a} is an added fluid mass per unit length accounting for the surrounding fluid, g is standard gravity, and c is the viscous damping coefficient. For an unconfined system such as this one, the viscous damping coefficient, c, is given by

$$c = \frac{2\sqrt{2}}{\sqrt{\mathrm{St}}}\Omega\rho_{\mathrm{f}} A_{\mathrm{e}}, \qquad (2)$$

where $\mathrm{St} = \Omega r_{\mathrm{o}}^2 / \nu$ is the Stokes number, $r_{\mathrm{o}} = \frac{1}{2} D_{\mathrm{o}}$, D_{o} is the outer diameter of the pipe, and ν is the kinematic viscosity of the surrounding quiescent fluid [3, 17]. Equation (1) is nearly identical to that for the discharging cantilever, save for the fact that U has been replaced with $-U$. From this point on, however, the special nature of the intake flow dynamics will be considered, and some changes to the equation will result.

First of all, the CFD simulations represented in Fig. 6 demonstrate that the flow in the vicinity of the free end for (a) the discharging pipe and (b) the aspirating pipe is quite different. In particular, Fig. 6(b) illustrates that the incoming flow at the inlet does not behave as a reverse jet; however, it is also clear that the aspirating inlet does not behave quite like a sink either. More concretely, Table 1 provides the values of the flow velocities and pressures just below, at, and just above the inlet, for a stationary cantilevered pipe aspirating air at 100 m/s. In the table, $(V_x)_{\mathrm{ave}}$ is the *average flow velocity in the negative x-direction*; V_{tot}, on the other hand, is the *average total flow velocity*. In addition, $\bar{p}$ is *pressure*, whereas $\bar{p}_{\mathrm{tot}}$ is *total* (or *stagnation*) *pressure*. By comparing the velocity at different locations, it can be seen that, as it enters the pipe, the fluid undergoes two distinct changes, translating into two distinct depressurizations.

Figure 7 illustrates more explicitly the different changes that occur as the flow enters the pipe, on a normalized scale. First, as the total flow velocity increases along a given streamline, a pressure drop occurs due exclusively to Bernoulli's equation. In Fig. 7, this can be seen by comparing the *average total velocity* (curve (2)) with the pressure loss calculated from Bernoulli's equation (curve (5)), and noticing that they reach their maxima simultaneously, just outside the inlet. This first depressurization, $\bar{p}_{\mathrm{intake}}$, is completed when the average total velocity becomes U, such that $\bar{p}_{\mathrm{intake}} = -\frac{1}{2}\rho U^2$. At this location, however, Fig. 7 also shows that the *average flow velocity in the negative x-direction* (curve (1)), $(V_x)_{\mathrm{ave}} \equiv v$, has not yet reached its maximum. More specifically, it is not U, but rather a large fraction of it, this because a certain portion of the flow is still entering from the sides. Consequently, as the final cross-flow components are eliminated between the inlet proper and a location just 1 mm further in, a second depressurization occurs, this time corresponding to a loss in total pressure (curve (4)), which is independent of the Bernoulli loss, as shown by Fig. 7. From the foregoing, it is clear that, although the average pressure (curve (3)) decreases at a fairly constant rate as the flow enters the pipe, the two pressure loss mechanisms are distinct and can be decoupled in order to model the inlet dynamics.

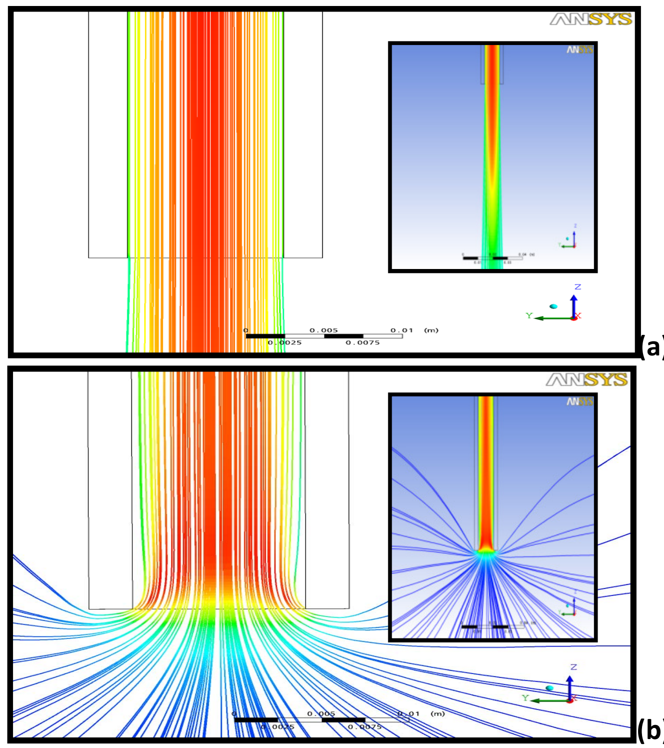

Figure 6. (a) Streamline plot for a discharging cantilevered pipe, near the free end. Inset: Streamline plot of the discharging jet-like flow, as seen from further away. **(b)** Streamline plot for an aspirating cantilevered pipe, near the free end. Inset: Streamline plot of the aspirating sink-like flow, as seen from further away. **Note:** The z-direction used in the plots corresponds to the negative x-direction in the theoretical model.

Table 1. Properties of the intake and inlet flow

Location versus inlet	$(V_x)_{\mathrm{ave}}$ (m/s)	V_{tot} (m/s)	$\bar{p}$ (Pa)	$\bar{p}_{\mathrm{tot}}$ (Pa)	$-\frac{1}{2}\rho V^2$ (Pa)
3 mm above	99	99	-1.1E+04	-3.9E+03	-5.8E+03
1 mm above	102	104	-1.1E+04	-3.4E+03	-6.4E+03
Inlet	88.1	102	-6.6E+03	-4.4E+02	-6.1E+03
1 mm below	28.8	48.7	-1.6E+03	2.4E+01	-1.4E+03
3 mm below	13.7	28.8	-5.0E+02	4.6E+01	-4.9E+02

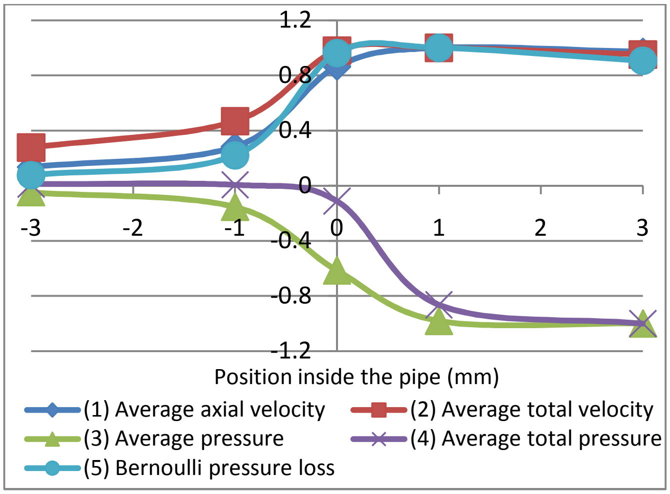

Figure 7. Normalized intake and inlet flow characteristics plotted versus position inside the pipe.

From the perspective of a 1-D approximation, based on the CFD analysis outlined above, we therefore state the following for the oscillating aspirating pipe: there exists a reduced velocity, v, tangential to the pipe and just facing the inlet, where a depressurization in accord with Bernoulli's equation, $\bar{p}_{\text{intake}} = -\frac{1}{2}\rho U^2$, as had been suggested by Kuiper and Metrikine [7], has already occurred. The pipe is, in general, inclined at an angle $\chi \equiv \tan^{-1}(\partial w/\partial x)_L \approx (\partial w/\partial x)_L$ with the vertical, as shown in Fig. 8(a), and the forces acting on the free end can be determined in both the (x, y) and (ξ, ζ) coordinate systems as shown in Fig.8(b). Moreover, as illustrated in Fig.8(c), the incoming flow velocity, v, is, in general, at an angle, ϑ, from the vertical, where we define ψ such that $\vartheta = \psi\chi$. In the case of air – and therefore in the present work – CFD analysis suggests that the two angles will be very close, satisfying $\psi \approx 0.90 - 1.00$.

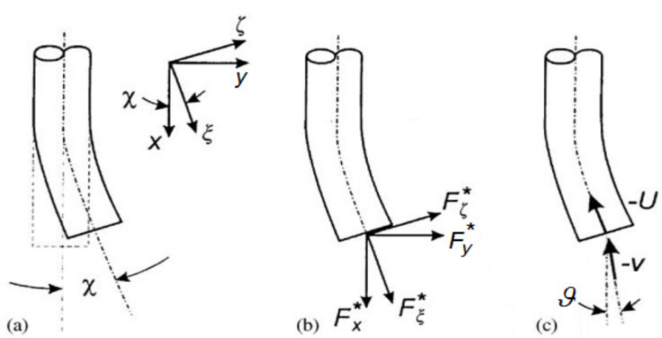

Figure 8. The free end of the pipe: **(a)** definition of the coordinate systems and the angle χ; **(b)** definition of the forces exerted by the fluid on the pipe; **(c)** definition of the mean flow velocity v and the angle ϑ; see Païdoussis *et al.* [8]

Under these assumptions, the force exerted by the pipe on the fluid in the x-direction is equal to the change in momentum of the fluid right at the inlet $MU(\Delta U)$, added to the effect of the pre-existing inlet depressurization, as follows:

$$F_x = MU[-U\cos\chi - (-v\cos\vartheta)] + \bar{p}_{\text{intake}} A\cos\chi. \tag{3}$$

In the y-direction, the force exerted by the pipe on the fluid is similarly due to the change in momentum, added to the lateral component of the inlet depressurization force, and can be written as

$$F_y = MU\{[(\partial w/\partial t)_L - U\sin\chi] - (-v\sin\vartheta)\} + \bar{p}_{\text{intake}} A\sin\chi. \tag{4}$$

Furthermore, assuming small deflections and therefore a small deflection angle, χ, we can approximate $\cos\chi \approx \cos\vartheta \approx 1$, $\sin\chi \approx \chi \approx (\partial w/\partial x)_L$ and $\sin\vartheta \approx \vartheta = \psi\chi \approx \psi(\partial w/\partial x)_L$, and Eqs. (3) and (4) simplify into

$$F_x = -MU^2(\tfrac{3}{2} - \alpha), \tag{5}$$

$$F_y = MU(\partial w/\partial t)_L - MU^2(\tfrac{3}{2} - \alpha\psi)(\partial w/\partial x)_L, \tag{6}$$

where $\bar{p}_{\text{intake}} A = -\frac{1}{2}\rho A U^2 = -\frac{1}{2}MU^2$ has been invoked, and $\alpha \equiv v/U$. Subsequently, Eqs. (5) and (6) may be manipulated in order to obtain the forces in the tilted (ξ, ζ) reference frame, and the signs inverted to express the forces exerted by the fluid on the pipe, F_ξ^* and F_ζ^*, as follows:

$$F_\xi^* \approx F_x^* = -F_x = MU^2(\tfrac{3}{2} - \alpha), \tag{7}$$

$$\begin{aligned} F_\zeta^* &= -F_\zeta \approx -F_y + F_x(\partial w/\partial x)_L = \\ &= -MU(\partial w/\partial t)_L + \alpha MU^2(1-\psi)(\partial w/\partial x)_L. \end{aligned} \tag{8}$$

It is now supposed that the depressurization force at the inlet is equal to the force exerted by the fluid on the pipe at the inlet in the ξ-direction, expressed as

$$-\bar{p}A = F_\xi^* \approx MU^2(\tfrac{3}{2} - \alpha). \tag{9}$$

Moreover, CFD analysis confirms the existence of a non-negligible average negative pressure on the lip of the pipe, related to the inlet depressurization and exerting a tension force, $\bar{T}$, on the pipe, as follows:

$$\overline{T} = -\gamma\overline{p}(A_e - A) = f\gamma MU^2(3/2 - \alpha) = \\ = \overline{\gamma}MU^2[(3/2 - \alpha)], \tag{10}$$

where $\gamma = \overline{p}_{\rm lip}/\overline{p}$, $\overline{\gamma} = f\gamma$, $f = (A_{\rm e} - A)/A$, and $A_{\rm e}$ is the total cross-sectional area of the pipe and fluid, as introduced by Païdoussis *et al.* [8]. Consequently, the term, $(\overline{T} - \overline{p}A)$, from Eq. (1), can be expressed as

$$(\overline{T} - \overline{p}A) = (1 + \overline{\gamma})(3/2 - \alpha)MU^2. \tag{11}$$

We next consider the boundary conditions on the aspirating pipe. At the clamped end, i.e. at $x = 0$, the boundary conditions are simply $w = \partial w/\partial x = 0$. At the free end, i.e. at $x = L$, the force in the lateral direction, F_ζ^*, must be accounted for, resulting in

$$EI\,\partial^2 w/\partial x^2 = 0, \\ EI\,\partial^3 w/\partial x^3 + MU(\partial w/\partial t)_L \\ -\alpha MU^2(1-\psi)(\partial w/\partial x)_L = 0; \tag{12}$$

the shear force boundary condition can be incorporated into the equation of motion via a Dirac delta function, $\delta(x - L)$ [3].

Finally, by combining Eqns. (1), (11) and (12), the equation of motion for a cantilevered pipe aspirating fluid can be obtained as follows:

$$EI\left[1 + \left(\overline{\alpha} + \frac{\overline{\mu}^*}{\Omega}\right)\frac{\partial}{\partial t}\right]\frac{\partial^4 w}{\partial x^4} \\ + \begin{Bmatrix}[1-(3/2-\alpha)(1+\overline{\gamma})]MU^2 \\ -(M+m-M_a)g(L-x)\end{Bmatrix}\frac{\partial^2 w}{\partial x^2} \\ +(M+m-M_a)g\frac{\partial w}{\partial x} - 2MU\frac{\partial^2 w}{\partial x \partial t} + c\frac{\partial w}{\partial t} \\ +(M+m+M_{\rm a})\frac{\partial^2 w}{\partial t^2} \\ + MU\left(\frac{\partial w}{\partial t} - \alpha U(1-\psi)\frac{\partial w}{\partial x}\right)\delta(x-L) = 0. \tag{13}$$

This equation can be rendered non-dimensional through the use of the dimensionless parameters

$$\xi = \frac{x}{L}, \quad \eta = \frac{w}{L}, \quad \tau = \left(\frac{EI}{M+m+M_a}\right)^{1/2}\frac{t}{L^2}, \tag{14}$$

yielding the dimensionless equation of motion

$$\left[1 + \left(\overline{\alpha}^* + \frac{\overline{\mu}^*}{\omega}\right)\frac{\partial}{\partial \tau}\right]\frac{\partial^4 \eta}{\partial \xi^4} \\ + \left\{[1-(3/2-\alpha)(1+\overline{\gamma})]u^2 - \gamma(1-\xi)\right\}\frac{\partial^2 \eta}{\partial \xi^2} \\ + \gamma\frac{\partial \eta}{\partial \xi} - 2\beta^{1/2}u\frac{\partial^2 \eta}{\partial \xi \partial \tau} + \sigma\frac{\partial \eta}{\partial \tau} + \frac{\partial^2 \eta}{\partial \tau^2} \\ + \left[\beta^{1/2}u\frac{\partial \eta}{\partial \tau} - \alpha(1-\psi)u^2\frac{\partial \eta}{\partial \xi}\right]\delta(\xi - 1) = 0, \tag{15}$$

in which the following non-dimensional parameters have arisen:

$$u = \left(\frac{M}{EI}\right)^{1/2}UL, \; \beta = \frac{M}{M+m+M_a}, \\ \gamma = \frac{(M+m-M_a)gL^3}{EI}, \; \overline{\alpha}^* = \left(\frac{EI}{M+m+M_a}\right)^{1/2}\frac{\overline{\alpha}}{L^2}, \\ \sigma = \frac{cL^2}{[EI(M+m+M_a)]^{1/2}}, \; \omega = \left(\frac{M+m+M_a}{EI}\right)^{1/2}\Omega L^2. \tag{16}$$

Finally, the equation is solved numerically using the Galerkin method in the form proposed by Païdoussis [3].

4.2 QUALITATIVE ANALYTICAL RESULTS

In the context of this study, parameters describing the inlet flow dynamics are assumed to fall into a limited range of values that are general for a wide range of pipes and flow velocities, established based on the CFD analysis; they are $\alpha \approx 0.7 - 0.9$ and $\overline{\gamma} \approx 0.30 - 0.40$. Moreover, the parameters used to model each pipe analytically are given in Table 2. In the case of the numerical simulations, the properties provided for Pipes A and B are exactly those modelled in ANSYS. In the case of the experiments, the fluid properties provided that depend heavily on density (M, M_a, and β) are based on local densities averaged over an entire run; the actual fluid properties vary with flow velocity. It should also be stressed that, although the numerical Pipe B was meant to replicate experiments as closely as possible, there are still small discrepancies between the two, as illustrated by Table 2. Therefore, quantitatively, they should not be directly compared; rather, results for each one must be compared with the analytical model.

Figure 9 displays the stability behaviour of the system for an illustrative set of fluid parameter choices. The top Argand diagram, which plots the imaginary part of the eigenfrequency versus the real part, shows that even very slight changes in the choice of parameters (in this case, varying ψ from 0.94 to 1.00) have a substantial effect on the behaviour of the system.

However, key trends do emerge. In the bottom right diagram, it can be seen that as the flow velocity is increased, the imaginary part of the eigenfrequency – and therefore the damping – at first remains relatively constant and near zero, suggesting the possibility for the same pendular motion captured in numerical simulations. Eventually, depending on the specific characteristics of the pipe under study, a flutter instability can occur through a Hopf bifurcation in the first mode. However, even past this point, the amount of negative damping (synonymous with an influx of energy) remains small, suggesting that the oscillations will be very weak, and easily damped out by any extraneous factors.

Table 2. Properties of the experimental and numerical simulation pipes, and critical flow velocities for the discharging case

Properties		Pipe 1	Pipe A	Pipe B
D_o	(m)	0.0159	0.0150	0.0159
D_i	(m)	0.00934	0.0100	0.00934
L	(m)	0.401	0.300	0.401
EI	(N·m^2)	7.63×10^{-3}	1.99×10^{-3}	7.63×10^{-3}
m	(kg/m)	0.144	9.82×10^{-3}	0.144
M	(kg/m)	8.81×10^{-5}	9.31×10^{-5}	8.12×10^{-5}
M_a	(kg/m)	3.01×10^{-4}	2.09×10^{-4}	2.34×10^{-4}
β	(-)	6.10×10^{-4}	9.20×10^{-3}	5.63×10^{-4}
γ	(-)	11.9	11.9	11.9
$\bar{\alpha}^*$	(-)	0.00030	2.40×10^{-3}	1.57×10^{-3}
$\bar{\mu}^*$	(-)	0.03578	0	0
f_1	(Hz)	1.27	4.43	1.27
δ_1	(-)	0.0423	N/A	0.0423
$(u_{crit})_{\mathrm{theo}}$	(-)	4.91	4.89	4.91
$(u_{crit})_{\mathrm{exp/num}}$	(-)	5.31	5.06	4.96

Therefore, in general terms, Fig. 9 demonstrates that the theoretical results for the numerical simulation Pipe B, agree with experiments and numerical simulations in predicting a very weak flutter instability. In particular, according to the theoretical model, the extremely limited amount of energy flowing into the system could explain why, in experiments, only an intermittent motion has been observed. Only for much greater flow velocities does the negative damping eventually increase considerably, potentially allowing for large oscillations; such velocities were not investigated in either experiments or numerical simulations, although larger oscillations were just beginning to emerge in both cases.

Similarly, for a sufficiently low value of ψ ($\psi \le 0.98$ for Pipe B, $\bar{\gamma} = 0.35$ and $\alpha = 0.8$) agreement is equally good when considering the real part of the eigenfrequency, i.e. the actual frequency of oscillation. Specifically, in both experiments and numerical simulations the frequency was found to stay relatively constant and decrease very slightly with flow velocity. Likewise, for an appropriate choice of parameters such as those used for Fig. 9, the theoretical model predicts that the frequency will indeed slowly decrease with flow velocity. Overall, experiments, numerical simulations and theory all predict the same type of behaviour.

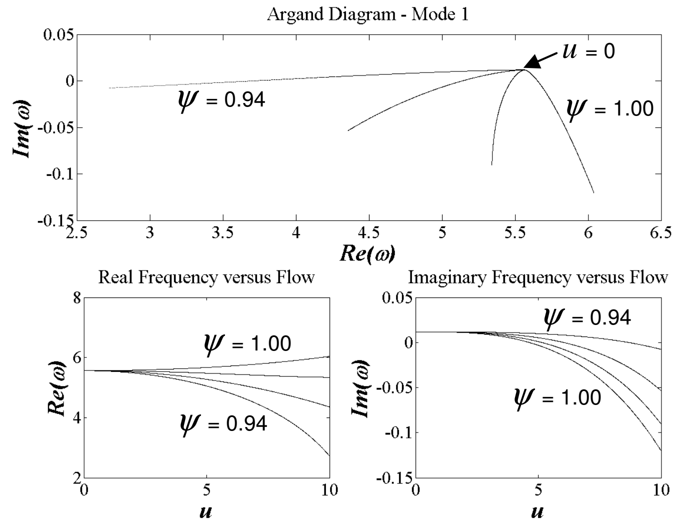

Figure 9. First mode Argand diagram, frequency and damping results produced by the theoretical modelling of numerical Pipe B; $\alpha = 0.8$, $\bar{\gamma} = 0.35$, ψ = 0.94, 0.96, 0.98 and 1.00.

5. QUANTITATIVE COMPARISON BETWEEN THE EXPERIMENTAL, NUMERICAL AND ANALYTICAL MODELS

Sections 2 to 4 have shown that, for the aspirating case in general, the exact value of the critical flow velocity is of lesser importance than in the discharging case, since the change in oscillation amplitude is not as dramatic, nor as potentially catastrophic. The theoretical model can indeed predict specific values for the threshold of flutter, but because of the flatness of the damping curve illustrated in Fig. 9, even a very large jump in critical flow velocity will only be reflected in a very small change in the dynamical behaviour. Consequently, in contrast to the discharging pipe, it is the qualitative behaviour of the aspirating pipe which is most important.

This contrast between the two configurations is made evident by comparing Figs. 10 and 11, which focus on the damping of the discharging and aspirating cases respectively. Figure 10 shows that, immediately after the pipe begins to flutter in its 2nd mode, the damping, $\mathrm{Im}(\omega)$, soon decreases from 0 to approximately -30. On the other hand, in the case of the aspirating pipe, Fig. 11 illustrates that the damping of the unstable 1st mode decreases from only 0 to just under -0.03, over a comparable range of flow velocities. Clearly, any small modification to the damping characteristics of the aspirating pipe makes a large quantitative difference that is not mirrored in the discharging case.

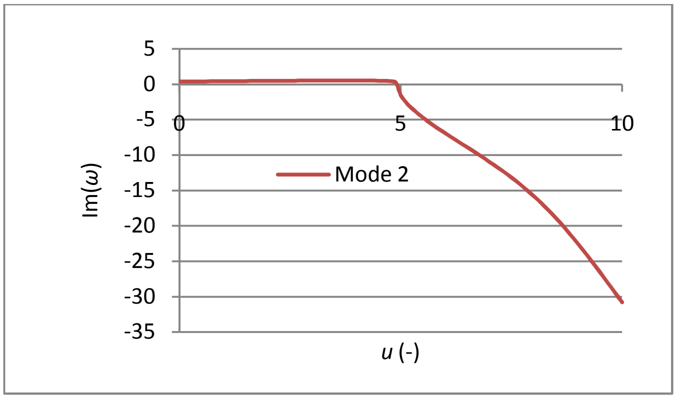

Figure 10. Theoretical eigenfrequency damping of the unstable 2nd mode plotted versus dimensionless flow velocity, for a discharging cantilever having properties similar to Pipe B.

Nevertheless, a limited choice of acceptable flow parameters produces a corresponding range of critical flow velocities which can be compared with estimates for the critical flow velocities obtained from the bifurcation curves for experiments and numerical simulations in Figs. 3(a) and 5 respectively. It must be noted, however, that this range is very large. Table 3 provides this comparison, illustrating adequate agreement, given the qualitative context: the extent of theoretical critical flow velocities encompasses the ranges estimated using the other two approaches. Furthermore, they are in the same mode, which is the first. From the foregoing, it therefore seems clear that, in the absence of sufficient damping, aspirating cantilevered pipes do indeed flutter at lower flow velocities than their discharging counterparts.

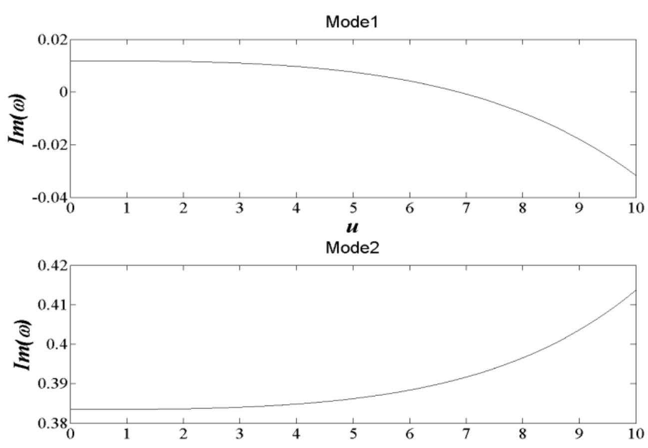

Figure 11. Theoretical eigenfrequency damping of the first two modes plotted versus dimensionless flow velocity, for an aspirating cantilever having the properties of Pipe B.

Table 3. Comparison of experiments and numerical simulation estimates for critical flow velocities with theoretical predictions

Pipe	Experimental Pipe 1	Numerical Pipe A	Numerical Pipe B
$(u_{\text{crit}})_{\text{experimental}}$	2.0 – 4.0	-	-
$(u_{\text{crit}})_{\text{numerical}}$	-	2.0 – 3.0	1.5 – 2.5
$(u_{\text{crit}})_{\text{analytical}}$	$\approx 2.0-5.0$, $(\alpha = 0.80\text{-}0.90,\ \ \psi = 0.96-1.00,\ \ \bar{\gamma} = 0.35)$ ‡		

6. CONCLUSION

This paper presented findings from experimental, numerical and analytical approaches to elucidate the question of whether aspirating cantilevered pipes flutter. This question, of a fundamental interest, has exercised researchers in the field of fluid-structure interactions for several decades, but has become all the more important with new applications emerging.

The evidence presented indicates that aspirating pipes do undergo a dynamic instability. However, because the instability is a very weak one, the strength of the conclusion can come only from corroboration between all three approaches. Indeed, the results all indicate that the aspirating pipe does flutter, but that the energy influx is very small, and therefore so too is the motion. The fact that numerous previous experiments did not suggest any self-excited oscillations reinforces this point. Altogether, it seems that, even though aspirating cantilevered pipes do indeed flutter at relatively small flow velocities, they clearly do not flutter very vigorously.

ACKNOWLEDGMENTS

The authors graciously acknowledge the financial support of the Natural Sciences and Engineering Research Council of Canada (NSERC).

REFERENCES

[1] Païdoussis, M.P. & Luu, T.P. (1985) "Dynamics of a Pipe Aspirating Fluid such as Might be Used in Ocean Mining." ASME Journal of Energy Resources Technology **107**, pp. 250–255.

[2] Giacobbi, D.B., Semler, C. & Païdoussis, M.P. (2008) "Numerical Fluid-Structure Interaction Study of a Cantilevered Pipe Discharging or Aspirating Fluid via a Computational Fluid Dynamics and Finite Element Analysis Model." Paper 48, *Proceedings of the 6th International Conference on Engineering Computational*

‡ These choices of parameters constitute a reasonable selection and thus provide a likely range of critical flow velocities. However, it must again be stressed that, because of the weakness of the instability, the exact value of critical flow velocity is much less important than the overall dynamical behavior, illustrated by Fig. 9.

Technology, ECT2008. 2-5 September 2008, Athens, Greece, ISBN 978-1-905088-25-6 CD-ROM, Civil Comp Press, Stirlingshire, Scotland.

[3] Païdoussis, M.P. (1998) *Fluid-Structure Interactions: Slender Structures and Axial Flow*, Volume 1. Academic Press Limited, London.

[4] Gleick, J. (1992) Genius: *The Life and Science of Richard Feynman*. Pantheon Books, New York.

[5] Païdoussis, M.P. & Tétreault-Friend, M. (2009) "Aspirating Cantilevers and Reverse Sprinklers." American Journal of Physics **77**, pp. 349-353.

[6] Païdoussis, M.P. (1999) "Aspirating Pipes do Not Flutter at Infinitesimally Small Flow." Journal of Fluids and Structures **13**, pp. 419–425.

[7] Kuiper, G.L. & Metrikine, A.V. (2005) "Dynamic Stability of a Submerged, Free-Hanging Riser Conveying Fluid." Journal of Sound and Vibration **280**, pp. 1051–1065.

[8] Païdoussis, M.P., Semler, C. & Wadham-Gagnon, M. (2005) "A Reappraisal of Why Aspirating Pipes do not Flutter at Infinitesimal Flow." Journal of Fluids and Structures **20**, pp. 147–156.

[9] Païdoussis, M.P. (2008a) "The Canonical Problem of the Fluid-Conveying Pipe and Radiation of the Knowledge Gained to Other Dynamics Problems across Applied Mechanics." Journal of Sound and Vibration **310**, pp. 462–492.

[10] Kuiper, G.L., Metrikine, A.V. & Efthymiou, M. (2007) "Experimental Investigation of the Dynamic Behaviour of a Water Intake Riser." *Proceedings of the 26th International Conference on Offshore Mechanics and Arctic Engineering*, *OMAE2007-29401*. 10-15 June 2007, San Diego, USA.

[11] Kuiper, G.L. & Metrikine, A.V. (2008) "Experimental Investigation of Dynamic Stability of a Cantilever Pipe Aspirating Fluid." Journal of Fluids and Structures **24**, pp. 541–558.

[12] Kuiper, G.L. (2008) "Stability of Offshore Risers Conveying Fluid." Ph.D. Thesis, Delft University of Technology.

[13] Rinaldi, S. (2009) "Experiments on the Dynamics of Cantilevered Pipes Subjected to Internal and/or External Axial Flow." M.Eng. Thesis, McGill University, Montreal.

[14] Giacobbi, D.B. (2007) "A Numerical and Experimental Study of the Dynamics of Aspirating Cantilever Pipes." B.Eng. Honours Thesis, McGill University, Montreal.

[15] Païdoussis, M.P. & Issid, N.T. (1974) "Dynamic stability of pipes conveying fluid." Journal of Sound and Vibration **33**, pp. 267–294.

[16] Païdoussis, M.P. & des Trois Maisons, P.E. (1971) "Free vibration of a heavy, damped, vertical cantilever." Journal of Applied Mechanics **38**, pp. 524–526.

[17] Batchelor, G.K. (1967) *An Introduction to Fluid Dynamics*. Cambridge University Press, Cambridge.